Graphical Abstract

Effect of pH and Surfactants on Shear Induced Asphaltene Removal

Syed Haider Abbas Rizvi, Shrimali Jonit Bharatbhai, Shivam Gupta, Jyoti Phirani, Vikram Singh

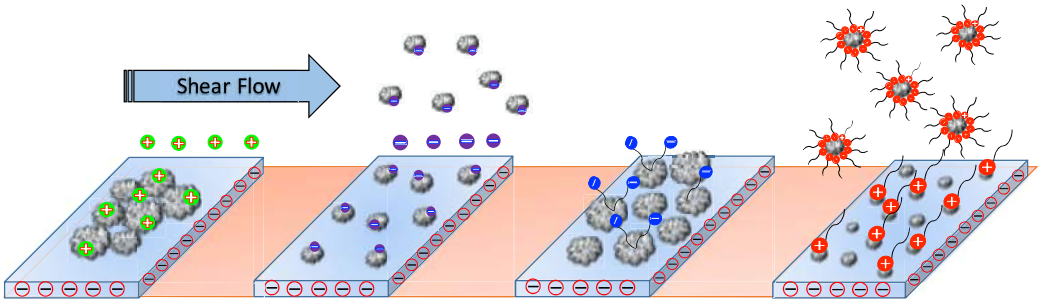

Highlights

Effect of pH and Surfactants on Shear Induced Asphaltene Removal

Syed Haider Abbas Rizvi, Shrimali Jonit Bharatbhai, Shivam Gupta, Jyoti Phirani, Vikram Singh

- Asphaltene removal through shear forces during water flooding is a reliable and non-destructive technique.
- Removal efficiency is also affected by effective zeta potential of asphaltene and surface in a medium.
- pH alterations and addition of ionic surfactants can enhance oil production, increase the bitumen recovery, and improve flow assurance.

Effect of pH and Surfactants on Shear Induced Asphaltene Removal

Syed Haider Abbas Rizvi, Shrimali Jonit Bharatbhai, Shivam Gupta, Jyoti Phirani, Vikram Singh*

Department of Chemical Engineering, Indian Institute of Technology, Delhi, New Delhi, India, 110016

Abstract

Asphaltene removal from sediments is essential for enhanced oil recovery from heavier crude oil reservoirs and tar sands and bitumen recovery from bottom products in downstream processes. Water injection or water flooding at high pressures exert shear forces that can overcome the adhesive forces between asphaltene and mineral surfaces. The adhesive forces are also affected by ions in the aqueous medium. In the current work we study asphaltene removal from silica surface using shear forces of aqueous media in a parallel plate channel. We demonstrate the effect of varying pH and surfactant conditions in aqueous media on asphaltene removal efficiency. We relate the removal efficiency with fractional asphaltene volume on the surface estimated from atomic force microscopy. The fractional asphaltene volume reduces to 0.12 at pH 10, which is approximately 50% lower than water at neutral pH at the same shear rate. We show that the water-soluble anionic surfactants are inefficient in asphaltene removal, whereas cationic surfactant reduces the asphaltene fraction to 0.30. We conclude that the removal efficiency is affected by the zeta potential of the asphaltene and the surface, where electrostatic repulsion between the asphaltene and the surface and increased wettability in the presence of cationic surfactant improves asphaltene removal.

Abbreviations: AFM, Atomic Force Microscopy; R_q, Root-mean-square Roughness; R_{max}, Maximum Height; Z_i, Height of Pixel; V_i, Volume of Pixel; V_t, Total Volume of Aggregates; $\bar{V}_t$, Normalized Volume

*Corresponding author

Email address: vs225@chemical.iitd.ac.in (Vikram Singh)

Keywords: Asphaltene, Deposition and Removal, pH Alterations, Sodium Dodecyl Sulfonate (SDS), Cetyltrimethylammonium Bromide (CTAB), Parallel Plate Channel, Atomic Force Microscopy (AFM)

1. Introduction

With an increased demand for oil on the global scale, heavier crude oils have captured the interest of the energy sector. The oil recovery from reservoirs can be enhanced by controlled salinity waterflooding (Collini et al., 2020; Wang et al., 2020); however, the process has challenges of water/oil emulsion formation (Rui et al., 2018; Taheri-Shakib et al., 2019b). The heavier crude oils have a considerable amount of asphaltene content (Ahmadi and Chen, 2020; Sjöblom et al., 2007) that deposits inside wells (Gharbi et al., 2017) and increase the gel point of wax crystals (Taheri-Shakib et al., 2020a,b). Scientists worldwide have constantly studied the onset of asphaltene precipitation and delaying the time of deposition (Kord et al., 2014; Soleymanzadeh et al., 2019; Vilas Bôas Fávero et al., 2016). However, asphaltene properties differ in lighter and heavier oils and are also based on their origin (Zojaji et al., 2021). Asphaltenes can solubilize in polar aromatic solvents like benzene or toluene (Mitchell and Speight, 1973; Yarranton, 1997), but the removal method is not cost-effective (Eskin et al., 2016; Salehzadeh et al., 2016). Hydrodynamic forces exerted by a fluid such as water can be a strategy to remove surface deposited asphaltene (Abbas Rizvi et al., 2021). The mitigation of asphaltene deposition is affected by system pH (Kar et al., 2020; Kesarwani et al., 2021), and effective use of surfactants (Hashmi and Firoozabadi, 2016; Ihtsham Hashmi and Ghosh, 2015; Keshavarz et al., 2019b). The hydrodynamic forces exerted by water injection at high pressures can effectively remove asphaltene deposits in the wells. Additionally, modification of aqueous media pH and dilution of ionic surfactants can impede the rate of asphaltene deposition and can cause their re-suspension in the bulk oil.

Asphaltenes are highly polar components of crude oil that contain aromatic and naphthenic groups along with N, S, and O as heteroatoms (Miadonye and Evans, 2010; Neil et al., 2015). The oil-suspended asphaltene molecules form colloids of sizes in a few hundred nanometers during the drilling processes as a result of the change in temperature, pressure, and oil composition (Indo et al., 2009; Mullins et al., 2012; Rajagopal and Silva,

2004). Larger asphaltene aggregates sediments or deposits on the surfaces in contact, primarily sand or silica, and consequently constricts the flow inside the pores (Scheffer et al., 2021; Taheri-Shakib et al., 2019a,b).

The oil suspended asphaltenes show electrokinetic behavior as a response to change in the zeta potentials. In the investigations carried out by Parra-Barraza et al. (2003) and Salmón-Vega et al. (2012) for zeta potential of asphaltenes as a function of pH, they suggested that asphaltene exhibit a positive charge at a lower pH and becomes negative as the pH increases. The positive zeta potential of asphaltenes at lower pH values attributes to the protonation of groups with nitrogen atoms. At a higher pH, the dissociation of acidic functional groups such as the carboxylic groups results in the negative zeta potential (Wang et al., 2009).

The charge exhibition by asphaltene molecules influences the interaction with surfaces in contact (Pradilla et al., 2016; Zhang et al., 2017). Also, the concentration of asphaltene elements (O, N, S) adhering to the surface affects the magnitude of zeta potential of asphaltene/mineral surface (Taheri-Shakib et al., 2018). Several other studies (Golsefatan and Shahbazi, 2020; Joonaki et al., 2019; Shayan and Mirzayi, 2015) have also reported that tuning the pH of aqueous media controls the adsorption and removal of asphaltene from the surfaces. Liu et al. (2020) reported that increasing pH lowers the adhesion force between asphaltene and silica that accelerates the desorption of asphaltene from the surface.

Ionic surfactants also have a coherent effect in altering the zeta potential that plays a vital role in the adsorption/desorption chemistry of asphaltene on a surface (Ahmadi and Chen, 2020; Alcázar-Vara, 2016; Lv et al., 2020). The effect is dependent on the charge on the asphaltenes (positive or negative) in the given system in the absence of any surfactant. Hashmi and Firoozabadi (2016) compared the efficiency of asphaltene solubilizing solvent toluene with an alkane soluble anionic surfactant dodecyl-benzene-sulfonic acid (DBSA). The removal of asphaltene deposits from stainless steel capillary tubes is observed, and the results suggest DBSA is as efficient as toluene. Al Sultan et al. (2018) also reports that DBSA efficiently removes the entire asphaltene from the glass beads. It is to be noted that DBSA is soluble in oil, and asphaltene removal from wells during water flooding might not be as efficient as expected with anionic surfactants. Madhi et al. (2018) compared the efficiencies of asphaltene removal in porous systems with several amphiphiles. The results suggest that cationic surfactant cetyltrimethylammonium bromide (CTAB) has higher removal efficiency for oil with more

negatively charged asphaltenes.

Kwon et al. (2018) suggest that adsorption of anionic surfactant occurs due to the interaction of alkyl chains of surfactants with hydrophobic sites of asphaltene. For cationic surfactants, the opposite polarity surfactant head groups facilitate the adsorption by lowering the zeta potential of colloidal asphaltene. Here, the adsorption increases proportionally with the length of the alkyl chain of the surfactant, where more extended chain surfactants adsorb more effectively on asphaltenes (Chang and Fogler, 1994; Wang et al., 2009). An essential aspect of surfactant adsorption on asphaltene surfaces is the concentration that affects the effective zeta potential of asphaltene-surface (LI et al., 2008).

In our previous study (Abbas Rizvi et al., 2021), we deposited asphaltene on glass slides from non-polar solvent heptane. We observed asphaltene removal from glass surfaces through hydrodynamic forces (mechanical removal). The asphaltene removal from substrates occurs in a parallel plate channel with water, where shear forces are tuned by controlling the flow rates. We compare the roughness of substrates at each step through atomic force microscopy. The decline in the roughness of asphaltene substrates as a function of shear forces is related to asphaltene removal. As an extension to our previous work, here in this study, we adopt an approach to remove surface asphaltene by pH alterations and ionic surfactants along with shear forces exerted in a parallel plate channel. The technique stated in the study shall be implemented during enhanced oil recovery with water flooding of reservoirs as well as downstream where water is added to the oil/bitumen slurry in the gravity separation vessels. The conditioning of aqueous media should affect the charge on asphaltene that causes them to re-suspend to the bulk. pH and surfactant addition in water reduce the damage to well-bore and the methods are cost-effective.

The current section stated the scope and importance of the project. The insights from the literature provide an overview of the effect of zeta potential to assist asphaltene removal. The following section (Section 2) defines the strategy and procedures for asphaltene extraction and deposition on the glass surface. We study the asphaltene removal in a parallel plate channel and observe the effect of pH and activity of water-soluble anionic and cationic surfactants. Section 3 shows the results of the experiments in terms of surface roughness (AFM) and fractional asphaltene volume on the surface. Section 4 concludes the study's findings, summarising significant outcomes and factors affecting the observations.

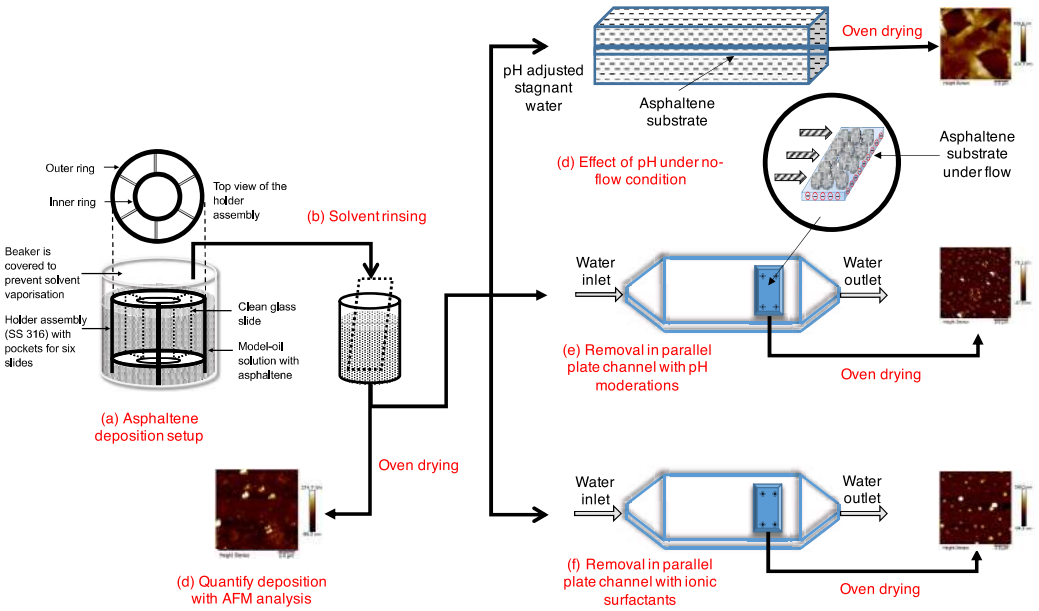

Figure 1: Process diagram: (a) asphaltene deposition on clean glass slides. (b) flushing the free asphaltene by dipping and removing immediately from three separate vials with pure solvent. (c) quantifying the extent of deposition after solvent rinsing using AFM. (d) solvent rinsed substrates are placed in *Stagnant* water at various pH values. (e) removal of asphaltene in parallel plate channel with pH alterations. (f) asphaltene removal employing ionic surfactants. The AFM analysis for either deposition or treatment with water is carried out after drying of substrate in oven for 24 h.

2. Methodology

Asphaltene is extracted from bitumen-kerosene emulsion (Shalibond, provided by STP Ltd) following the standard ASTM D2007-80 procedure using the *n*-heptane (HPLC grade, Fisher Scientific) in Soxhlet extractor (Al-Sahhaf et al., 2002; Alboudwarej et al., 2002). The filtered contents from the extractor are treated with toluene (HPLC grade, Fisher Scientific) and vacuum dried to obtain asphaltene. Figure 1 shows a schematic process that briefs the rest of the experimental procedure followed in the study. The deposition of asphaltene on pre-cleaned glass slides is carried out in an asphaltene/heptane model-oil system through 24 h of aging at definite temperatures with stirring (Figure 1a). The substrates are dipped and immediately taken out from three separate vials that contain pure heptane (Figure 1b). This additional step prevents inconsistent results caused by the unadsorbed

asphaltene on the surface. We quantify the extent of deposition (Figure 1c) after solvent rinsing and oven drying for 24 h using an atomic force microscope (AFM). In a separate set of experiments, the heptane rinsed substrates are directly treated with water under desired conditions. We first evaluate the effect of water under zero flow or *Stagnant* condition with pH alterations (Figure 1d). A fresh set of solvent rinsed substrates observes asphaltene removal in a parallel plate channel. As a function of shear rates, the removal efficiency is compared in separate experiments by altering the pH of aqueous media (Figure 1e) and through the use of ionic surfactants (Figure 1f). We select anionic sodium dodecyl sulfonate, SDS (Fisher Scientific) and cationic cetyltrimethylammonium bromide, CTAB (Fisher Scientific) as surfactants for this study. At the last step after water treatment, the substrates are dried in an oven and then analyzed for surface morphology from AFM. It is to be noted that no pre-characterization (AFM analysis) is carried out on a glass slide sent to the parallel plate channel.

2.1. Preparation of Substrates

Borosilicate glass is widely accepted as proxy surface for silica and has over 80% SiO_2 (Kumar et al., 2008). The deposition of asphaltene is carried out on microscopic glass slides (75 $\times$ 25 mm) to mimic asphaltene deposition on silica surfaces (Ratnakar et al., 2020; Soorghali et al., 2015). Before the asphaltene deposition, the glass slides are rinsed properly with surfactant solution (Teepol, CDH Fine Chemicals) followed by DI water about three to four times to ensure removal of oil and dirt. The glass slides are further sonicated with iso-propanol (Fischer Scientific) and DI water for 10 min in each and dried with nitrogen in the end. We validate that the glass slides are free of any surfactant by observing the water contact angles lesser than 5° (Sumner et al., 2004).

Asphaltene is deposited on clean glass slides in a batch system containing heptane with 0.03 g/L asphaltene. The asphaltenes are first dispersed in toluene in the ratio 4:1 w/v and sonicated for 60 min. The net contents are added to heptane in a beaker maintaining the stated concentration. The clean glass slides, six at a time, are held upright in a stainless steel holder. The glass slides are immersed in the asphaltene-heptane dispersion such that the slides are below the free surface of the liquid. The beaker is covered from the top, and the system is kept for stirring at 450 rpm for 24 h at 90°C to observe deposition of asphaltene. The elevated temperatures facilitate the suspension of asphaltene and prevent sedimentation in dead zones during

stirring. After the aging, the substrates are rinsed with heptane to flush out the free asphaltene in the film. To quantify our deposition results, we dry the substrates and characterize them with AFM at this stage.

2.2. Application of Hydrodynamic Force in Parallel Plate Channel

We observe the removal of asphaltene from the substrates by applying hydrodynamic force with water in a parallel plate channel Abbas Rizvi et al. (2021). The channel is fabricated from stainless steel (SS316) with a pocket to place two glass slides adjacent. A rectangular cap covers the pocket, tightened with screws to avoid leakage. The water flows through stainless steel tubings, regulated by control valves. The calculation of shear rates is from ANSYS Fluent simulations employing $\kappa - \epsilon$ turbulent flow model. We observe removal at five shear rates, 1.23×10^3 s^{-1}, 3.03×10^3 s^{-1}, 5.46×10^3 s^{-1}, 1.69×10^4 s^{-1}, 2.37×10^4 s^{-1}, including a no-flow or *Stagnant* state.

For every shear rate (separate experiment), the flow setup operates for 20 min after substrate placement in the channel. We tune the water pH at the beginning of the experiment by adding 0.1 N hydrochloric acid (Merck) or 1 N sodium hydroxide solution (Merck) as per the experimental requirements. While using the surfactants SDS and CTAB, the setup is initially operated blank (without substrate) for 30 min to dissolve surfactants properly.

2.3. Atomic Force Microscopy

At the end of the experiments, the substrates are dried for 24 h at 90°C in a hot air oven. We characterize the substrates through AFM, and these substrates are not further used in any experiments. A Bruker Dimension Icon AFM maps the surface in *Tapping in Air* mode, creating images of 10 μm $\times$ 10 μm at a frequency of 0.804 Hz. Each scan records the pixel information in a 512 $\times$ 512 matrix, producing *height sensor* and *phase* images. The *height sensor* images show morphological information of the surface. The *phase* images have contrast based on the material's stiffness properties reflected as phase angles. A homogeneous surface has even contrast and a relatively narrower range of phase angles. We carry out the image analysis using Bruker's Nanoscope Analysis software. The results are expressed as root-mean-square roughness (R_q), and the distance between the highest and the lowest point calculated using a datum line (R_{max}). Apart from these parameters, the cross-section analysis, from the *Section Analysis* tool, gives pixel-wise information about the fraction of asphaltene on the substrates. The details about the procedures can be found in Appendix Appendix B.1.

2.4. Zeta Potential Measurements

The Zetasizer Nano ZSP (Malvern Panalytical) records the zeta potential, taking three readings per sample. We adopt the process stated in the study by Grijalva-Monteverde et al. (2005) for estimation of zeta potential of asphaltene in polar fractions. The stock solution is a dispersion of asphaltene in water prepared by sonicating 50 mg of asphaltene in 15 mL of ethanol for 60 minutes. Ethanol is a poor solvent for asphaltene but preferred over toluene due to its miscibility in water (Ok et al., 2019). During the zeta potential measurements, 1.5 mL of stock solution is purged into 100 mL of DI water whose ionic strength is fixated by dissolving 1 mM $NaNO_3$ (Merck). The pH is altered using 0.1 N HCl to prepare acidic solutions or 1 N NaOH to prepare basic conditions. While recording zeta potentials with ionic surfactants, concentrations of SDS and CTAB are varied from 0.1 - 1.0 wt.%.

3. Results and Discussion

On the clean glass slides, we report a roughness of 0.3 nm and phase angles within $\pm 2^{\circ}$. Asphaltene deposition on these slides occurs from a heptane-asphaltene dispersion via aging. The increase in the roughness and phase angle confirms the deposition of asphaltene on the surface (Cheng et al., 2008; Scott and Bhushan, 2003). The asphaltene substrates are exposed to hydrodynamic forces in a parallel plate channel to observe asphaltene removal. We compare the efficiency of removal as a function of shear rates and net zeta potential of the system upon pH alterations or the addition of surfactants. We quantify our results as the change in the roughness of substrates and fractional asphaltene volume on the surface.

3.1. Asphaltene Deposition

The asphaltene-aged substrates (post 24 h deposition) are rinsed with heptane to minimize errors caused by non-deposited asphaltene in the film. This rinsing is done in three separate vials containing pure heptane. The AFM images of one such substrate are shown in Figure 2. We report that the mean roughness from eight similar deposition experiments is 34.9 ± 3 nm. The *phase* images also show wider phase angles with visual contrast throughout the entire scans. The darker regions are of lesser stiffness representing asphaltene, and the glass surface is depicted by lighter contrast of higher stiffness.

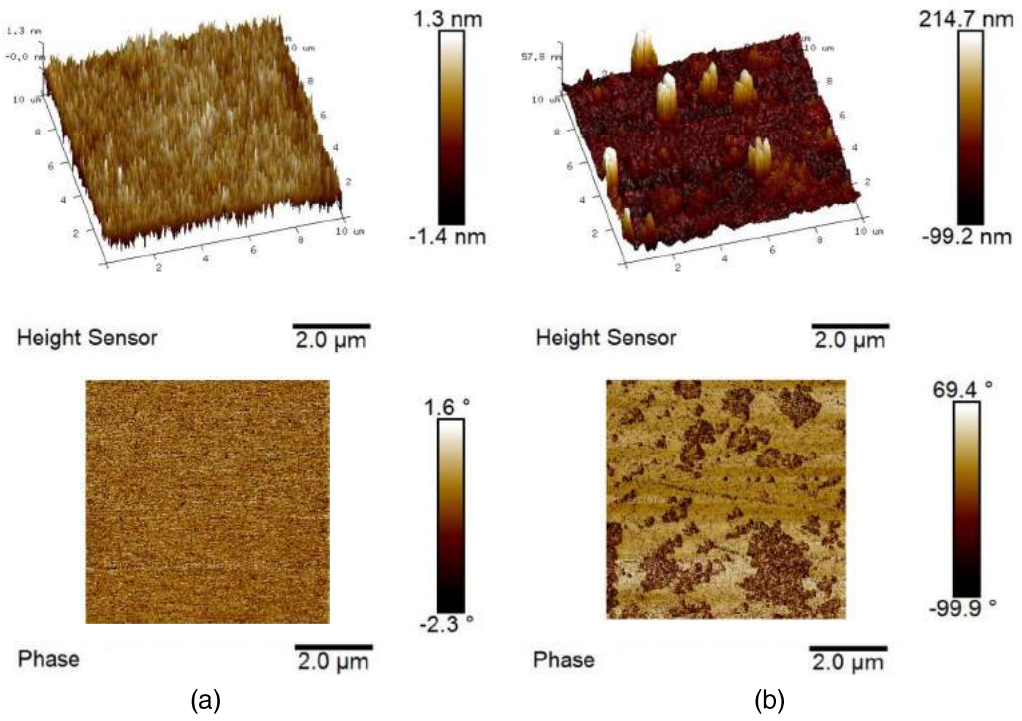

Figure 2: The *height sensor* and *phase* images of (a) clean glass slide, and (b) heptane rinsed substrate. After the deposition of asphaltene the surface roughness of substrate increases to 37.49 nm. The *phase* images have relatively broad range of phase angles along with visible contrast. The dark patches represent asphaltene deposition.

3.2. Substrates in contact with Stagnant water - Effect of pH at Zero Flow

The asphaltene-aged substrates rinsed with heptane are kept in 50 ml vials for 20 minutes at the desired pH. This step can also be performed in the parallel plate channel for a *Stagnant* (zero flow) state. However, we avoid carrying out the experiments in the channel because of the corrosion effects on steel in acidic medium/presence of Cl^- ion. Therefore, for ease of discussion, these substrates are also referred to as *Stagnant*.

The *height sensor* images of *Stagnant* substrates at various water pH are shown in Figure 3. The morphology of substrates at low pH values suggests widespread asphaltene aggregation on the surfaces. As the pH increases, the aggregates seem to be rather disintegrated.

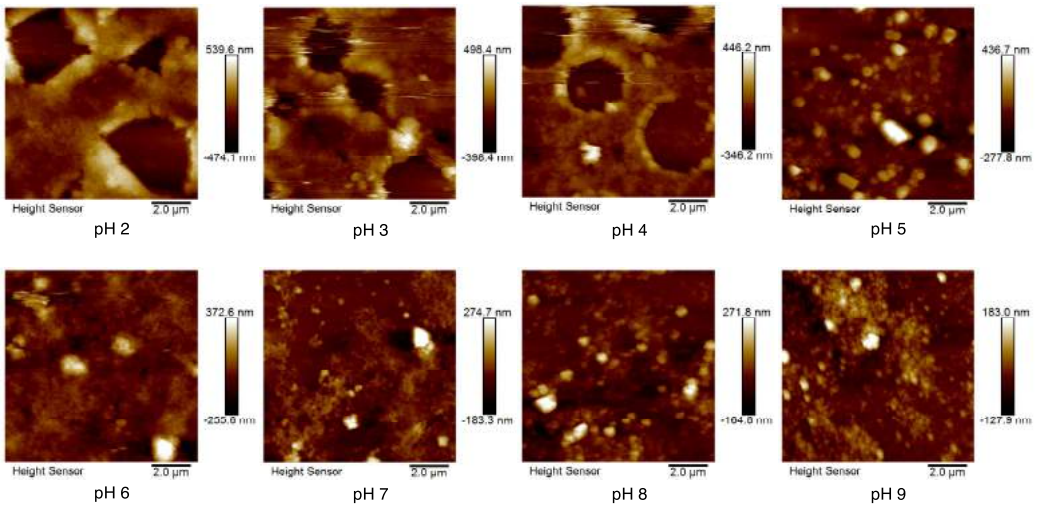

Figure 3: The *height sensor* images of *Stagnant* substrates at various pH values in water. The scale bars on the right represent the height of maximum and minimum points on scan.

Figure 4(a) and (b) reports the roughness and maximum height of aggregates for *Stagnant* substrates as a function of aqueous media pH. An important observation here is that roughness at all pH values is higher than the heptane rinsed substrate ($\approx$ 35 nm). The diffusion of water molecules causes reorientation of hydrophobic chains within asphaltene aggregates and results in swelled structures (Abraham et al., 2002; Zhang et al., 2017). We also observe the effect of time for which the substrates are exposed in water. Asphaltenes substrates are kept at the desired pH for 1 m, 20 m, and 24 h in three separate vials. After the 24 h drying process, the substrates are analyzed through AFM. We find that the roughness is similar for all the specimens, suggesting that the reorientation is an almost instantaneous process or at least occurs at time scales much less than $O(1\text{ m})$.

The size of asphaltene aggregates is greatly affected by the electrostatic double-layer charges in the system. We measure the zeta potentials for asphaltene dispersed in DI water at different pH values that are mentioned in Figure 5(a). At lower pH values till pH 5, the zeta potential has a positive value. The iso-electric point (IEP) in our study lies at pH 5.2. For higher pH, the zeta potential values decrease. For silica glass, the literature reports the zeta potentials as a function of pH and suggests negative values at pH 2, increasing in the negative direction as the alkalinity increases (Andrade et al.,

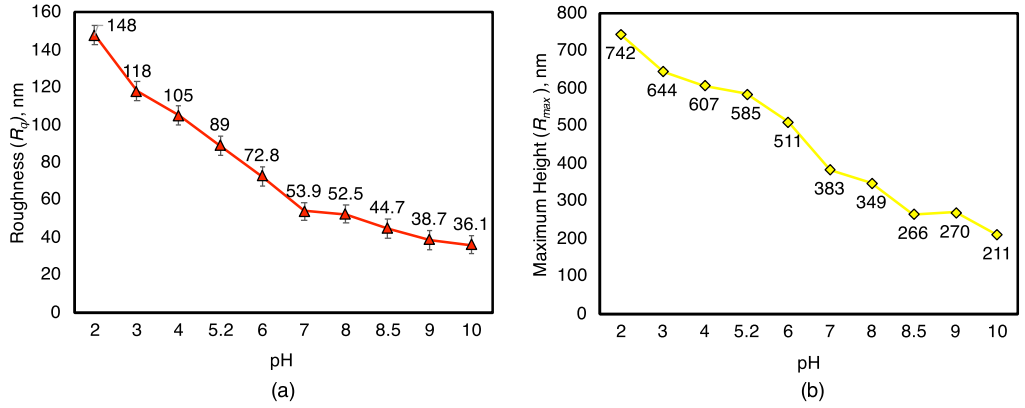

Figure 4: (a) root mean square roughness, R_q (▲), and (b) maximum height, R_{max} (◆) for *Stagnant* substrates in contact with water at different pH conditions.

2009; Gu and Li, 2000). Taheri-Shakib et al. (2018) states that asphaltene adsorption on sandstone/silica is promoted by the accumulation of O and S elements that negatively increase the effective zeta potential. Dolomite surfaces depict a similar characteristics with S elements of asphaltene, resulting in strong adherence of asphaltene to the surface (Taheri-Shakib et al., 2019a).

Long et al. (2007) reports the existence of longer asphaltene aggregates in an acidic medium. As the zeta potentials approach negative values, the electrostatic repulsion between asphaltene aggregates breaks the larger aggregates into smaller ones. The alkyl chains in asphaltenes tend to coil easily at lower pH values but can have an extended structure in an alkaline solution. Nonetheless, in an acidic medium, increased number of -NH^+ and >SiO^- bonds also result in strong adhesion between asphaltenes and silica surface (Liu et al., 2020), affecting the morphology and roughness of substrates (Figure 4(a)).

We verify our results by estimating the volume of asphaltene on the surface as shown in Figure 5(b). The AFM scans of the substrate are analyzed using the *Section Analysis* tool on the software. Several lines are sketched across the image to extract information from 5530 pixels of the scan. We obtain the volume (V_i) of asphaltene deposited on each pixel by multiplying that pixel's height with the area occupied by a single pixel. We further normalize the total volume (V_t) at a specific pH with respect to the volume of asphaltene ($V_t|_{pH7}$) deposited on the substrate at the zero shear rate and $pH = 7$. The total normalized volume ($\bar{V}_t$) at a shear rate is given by

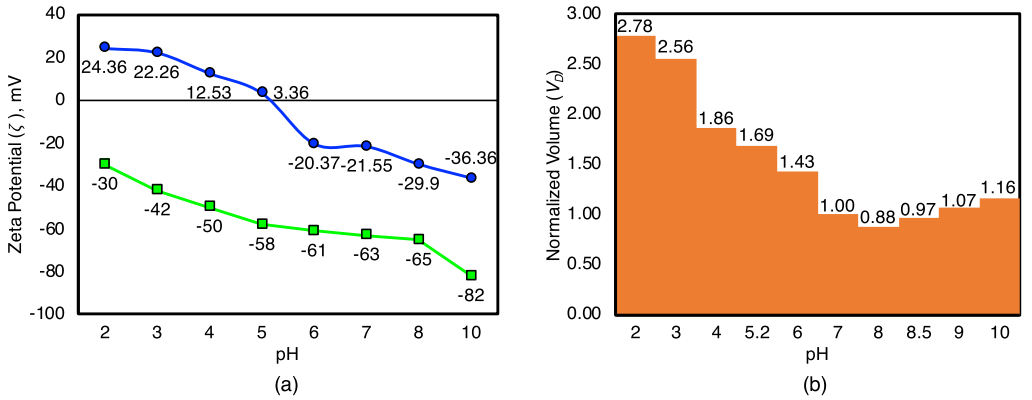

Figure 5: (a) zeta potential of asphaltene (●) and glass (■) in water as a function of pH. For glass, the estimated zeta potentials are from the study conducted by Gu and Li (2000). (b) normalized asphaltene volume on *Stagnant* substrates at various pH values. The normalization is done by total volume of aggregates on the surface at pH 7.

equation 1,

$$\bar{V}_t = V_t / V_t|_{pH7} \tag{1}$$

In Figure 5(b), we observe that increasing the pH starting at 2, $\bar{V}_t$ decreases as the number of excess H^+ reduces, and the aggregation increases again beyond pH 8.5. Asphaltenes are relatively much polar than other hydrocarbons, and their wettability is towards oil-wet. Elsharkawy et al. (2008) state that acidic and basic functional groups are differently ionized at different pH, and their surface activity is a function of pH (Figure 6(a)). It is most strongly affected at the extremes of low pH (2–4) and high pH (8–10). The effect is more substantial in the high pH range for asphaltenes that contain more acidic groups than basic groups (Poteau et al., 2005). However, in our case, the swelling is more prominent in the acidic regime. The excess H^+ ions in the acidic medium form hydrogen bonds with nitrogen atoms of asphaltene (Guo et al., 2020), and tends to change the asphaltene wettability from oil-wet to more water-wet (Figure 6(b)). The phenomenon is conventional in higher pH ranges where $-COO^-$ forms a cooperative system with water molecules and acquires slight hydrophilicity (Figure 6(c)). We give a plausible explanation that higher diffusion of water molecules due to enhanced hydrophilicity causes more significant swelling of asphaltene aggregates, observed as increased $\bar{V}_t$ in our study.

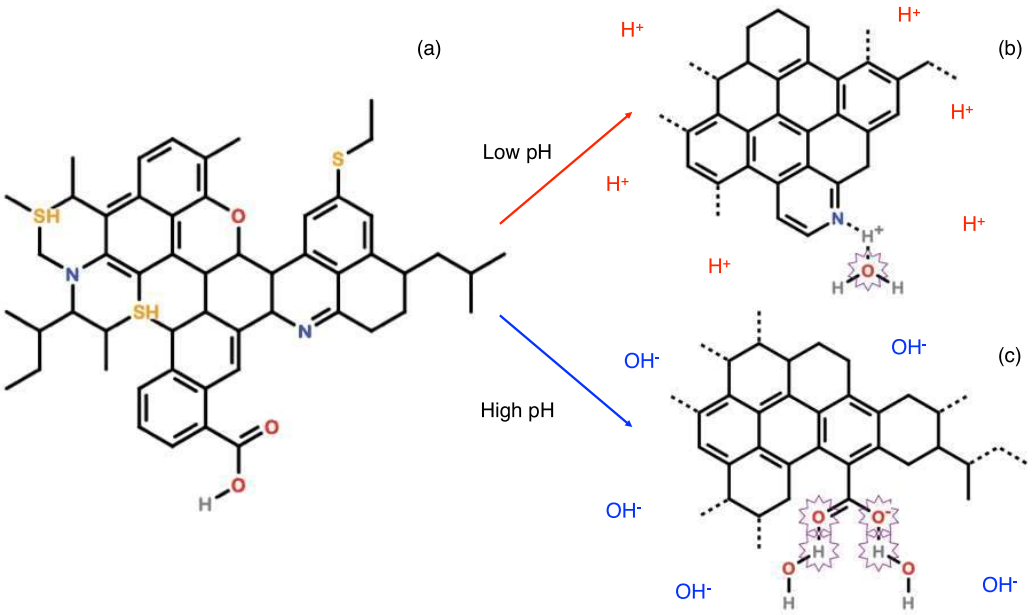

Figure 6: (a) illustration of an asphaltene molecule (Fakher et al., 2020). The aromatic rings are fused with alkyl chains attached to the structure. Both acidic and basic groups can functionalize at extreme pH by forming hydrogen bonds with water, resulting in swelling of aggregates. (b) the protonation of nitrogen-containing groups at low pH results in positive zeta potential and increased affinity for water. (c) in an alkaline medium, the polarization of carboxylic groups causes negative zeta potential and increased hydrophilicity of asphaltene.

3.3. Asphaltene Removal by Hydrodynamic Forces with pH alterations

We previously observed the asphaltene removal as a function of shear rates where reduction in roughness infers removal from the surface. We observe six different shear rates: *Stagnant* (zero), 1.23×10^3 s^{-1}, 3.03×10^3 s^{-1}, 5.46×10^3 s^{-1}, 1.69×10^4 s^{-1}, and 2.37×10^4 s^{-1}. Here in this study, the effect of shear rates is observed at four different pH values of aqueous media - pH 5.2 (IEP), pH 7, pH 8.5, and pH 10. The mean values of roughness from eight sets of experiments are shown in Figure 7.

At a pH of 5.2, i.e., the iso-electric point for asphaltene dispersion in water, the asphaltene aggregates firmly adhere to the substrates. There is a further increase in roughness at the next higher value of shear rate (1.23×10^3 s^{-1}). In the initial stages of shear rates, the rearrangement of aggregates occurs due to lower hydrodynamic forces. Some of the loosely

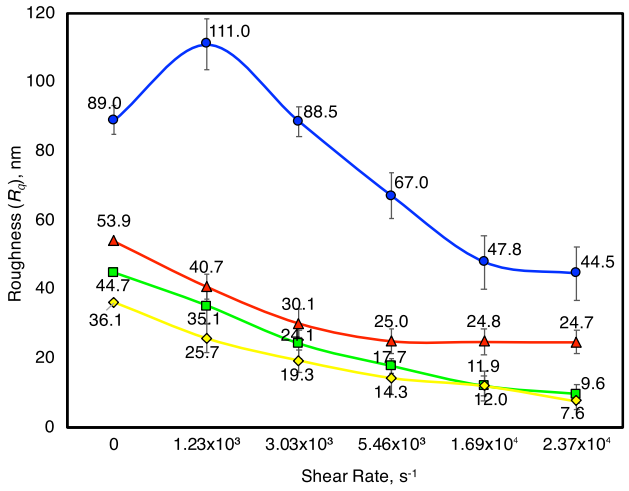

Figure 7: The mean roughness (eight experiments) of substrates as a function of shear rates when pH is altered during removal experiments. The curves are: pH 5.2 (●), pH 7 (▲), pH 8.5 (■), and pH 10 (◆).

adhered aggregates migrated to relatively larger aggregates, which further increased their size, and hence greater roughness is observed. With further increase in the shear rates, the roughness declines to a value of ∼45 nm, which is still higher than those of heptane rinsed substrates.

In all other experiments at the other three pH values, the roughness varied inversely with the shear rates. As the pH increases from 7 to 8.5, the electrostatic double layer repulsion between asphaltene and silica increases, which favors the asphaltene desorption from the surface (Liu et al., 2020). For pH 10, the roughness significantly reduced from 36±2 nm to ∼8 nm at the highest offered shear rate of 2.37×10^4 s^{-1}. The *height sensor* and *phase* images from an experiment at pH 10 are shown in Figure B.12. We approximate the normalized volume of asphaltene on the substrate ($\bar{V}_t$) by using the same approach as mentioned above section. We define the fractional asphaltene volume that remain after application of hydrodynamic forces in equation 2,

$$\bar{V}_{treduced} = \frac{\bar{V}_t|_{\text{max shear}}}{\bar{V}_t|_{Stagnant}} \tag{2}$$

The fractional volume of asphaltene estimated from the above expression ($\bar{V}_{treduced}$) at various pH values is 0.36 at pH 5.2, 0.24 at pH 7, 0.21 at pH 8.5,

and 0.12 at pH 10, respectively. These inferences suggest that the asphaltene removal is affected by the hydrodynamic forces and the pH of the media. The plots for the normalized asphaltene volume under the influence of shear forces at various pH values are shown in Figure C.14.

It is important to note that electrostatic interactions are affected by the heteroatom concentration in asphaltenes. Asphaltenes differing in origins will show the different extent of deposition affected by the surrounding medium (solvent). Similarly, asphaltene removal depends on the solvency potential and ions in the medium. Also, it has been reported that reduction in -NH and -OH bonds between asphaltene and surface, either by chemical solvents (Keshavarz et al., 2019a,b) or pH alterations (Liu et al., 2020) will increase asphaltene removal.

3.4. Activity of Ionic Surfactants on Asphaltene Removal

The effect of anionic and cationic surfactants on the efficiency of asphaltene removal is tested in this set of experiments. The anionic surfactants show little affinity towards negatively charged silica surfaces resulting in a non-adhesive system. Only slight adsorption of SDS is reported by Li and Ishiguro (2016) where at high concentrations, the hydrophobic tail of the surfactant might interact with the silica surface. The cationic surfactants, on the other hand, render the glass surfaces with a net positive charge for surfactant concentration above 10^{-3} M (Gu and Li, 2000). The cationic surfactants adsorb on silica resulting in concentration-dependent interactions, where negatively charged surfaces interact with cationic surfactants due to electrostatic interactions forming monolayer or bilayer structures (Rapp et al., 2015; Tyrode et al., 2008). The adsorbed surfactant is expected to improve the wetting properties of the silica surface.

Several scientists have studied the zeta potentials of asphaltene in the presence of ionic surfactants. The initial polarity of zeta potentials for asphaltene affects the net charge when ionic surfactants are adsorbed on the surface (Leon et al., 2000; Neves et al., 2001; Parra-Barraza et al., 2003; Wang et al., 2009). We measure the zeta potential of asphaltene dispersed in ethanol, purged in aqueous solutions of ionic surfactants at neutral pH. The zeta potentials of asphaltene as a function of surfactant concentration from 0.1 - 1.0 wt.% are shown in Figure 8(a).

The zeta potential instantly increased in the negative direction, maintaining a similar value for all concentrations of SDS from 0.1 to 1.0 wt.%. The

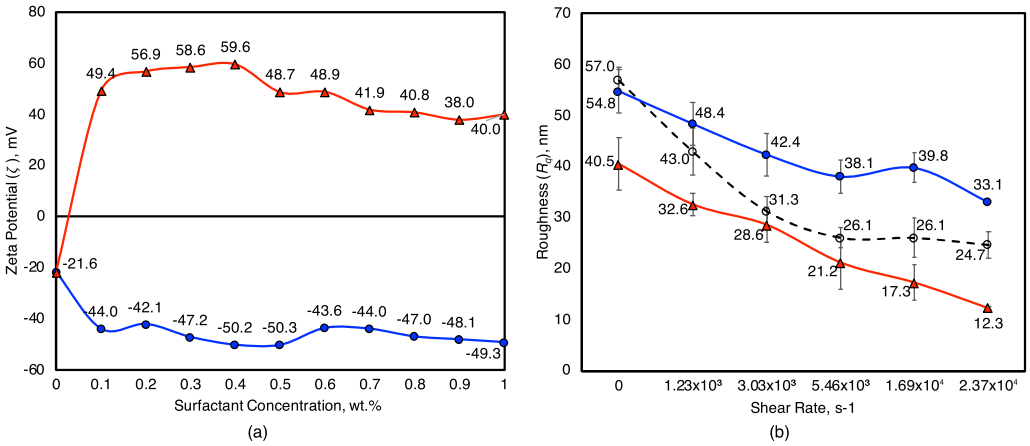

Figure 8: (a) zeta potential of asphaltene in water as a function of SDS (—) and CTAB (—) concentration at neutral pH. (b) roughness of asphaltene substrates as function of shear rates with 0.5 wt% SDS (—), 0.4 wt% CTAB (—), and no surfactant (- -).

maximum zeta potential, ∼-50 mV, is recorded at 0.5 wt.% of SDS, approximating at twice its critical micelle concentration (8.2 mM). The increase in zeta potential is due to the adsorption of SDS on asphaltene with hydrophobic interactions (LI et al., 2008; Salmón-Vega et al., 2012). We observe a sharp increase in zeta potential in the positive direction for asphaltene in the presence of cationic surfactant CTAB. Wang et al. (2009) have found that amphiphiles' adsorption on oppositely charged asphaltenes occurs through acid-base interaction or electrostatic interaction, which might result in neutralization of surface charges. The concentration of CTAB (0.4 wt.% ≈ 12 times higher than the CMC) in the current study is sufficiently high for the asphaltenes-CTAB complex to exhibit zeta potentials as high as ∼+60 mV. Singh (1999) observed the surface properties of another organic substrate (coal) in the presence of both anionic and cationic surfactants. The author found that the increased adsorption of cationic surfactant on the negatively charged coal surface affects the interfacial energy, resulting in the coal substrate becoming more water-wet. The coal surface has a large contact angle in the presence of anionic surfactants.

We carry out the asphaltene removal from the silica surfaces at the highest recorded zeta potentials obtained for respective surfactants, i.e., at 0.5 wt.% SDS and 0.4 wt.% CTAB. Figure 8(b) shows the results for roughness as a function of shear rates with surfactants at neutral pH.

3.4.1. Removal with Anionic Surfactant (SDS)

As evident from Figure 8(b), the asphaltene substrates' roughness appears on a higher value for the same shear rates with sodium dodecyl sulfate than without any surfactant at all. The roughness shows a marginal decline at *Stagnant* state due to the separation of some of the asphaltene aggregates along with the surfactant, which gradually decreases as a function of increasing shear rate. However, these values are comparably higher than those in the absence of surfactants. The reduction in roughness occurs only due to high magnitudes of shear forces. These observations are contrary to the results for asphaltene removal at high pH discussed earlier, where an increase in asphaltene zeta potential results in removal. The literature cites stable adsorption of asphaltene aggregates due to the hydrophobic interactions with the anionic amphiphiles, and we suggest similar phenomena occurring at the surface (Kwon et al., 2018; Parra-Barraza et al., 2003; Salmón-Vega et al., 2012). Figure 9(a) and Figure 9(b) shows AFM images of substrates at zero shear rate and 2.37×10^4 s^{-1} with 0.5 wt.% SDS. Referring to the top *height sensor* images, it appears that the relative roughness has decreased with the shear rate, but there are aggregates with comparable sizes on the surface. The *phase* images at both these shear rates provide evidence for significant asphaltene coverage on the surface.

3.4.2. Removal with Cationic Surfactant (CTAB)

In the presence of the cationic surfactant CTAB, the efficiency of removal has significantly increased (Figure 8b). The *Stagnant* state substrates show a significant reduction in the roughness of approximately 40.5±5 nm. Further reduction in roughness is observed as a function of increasing shear rates, attaining a value of ≈12 nm.

The AFM *height sensor* and *phase* images of substrates at *Stagnant* and 2.37×10^4 s^{-1} are shown in Figure 10. We observe that asphaltene from the low concentrated areas has already been removed even without the flow. The removal significantly enhances when hydrodynamic forces are applied. As evident from images at 2.37×10^4 s^{-1}, the large aggregates have weathered and removed along with the flow. The *phase* image at this shear rate also depicts amplified lighter contrast signifying cleaner substrate. Adsorption of CTAB on both the asphaltene and the silica surface has been shown to lower the water-substrate surface tension (Singh, 1999). The formation of a solvation envelope around the asphaltene promotes their surface desorption and dissolution in the medium (León et al., 1999; Rogel et al., 2001). The

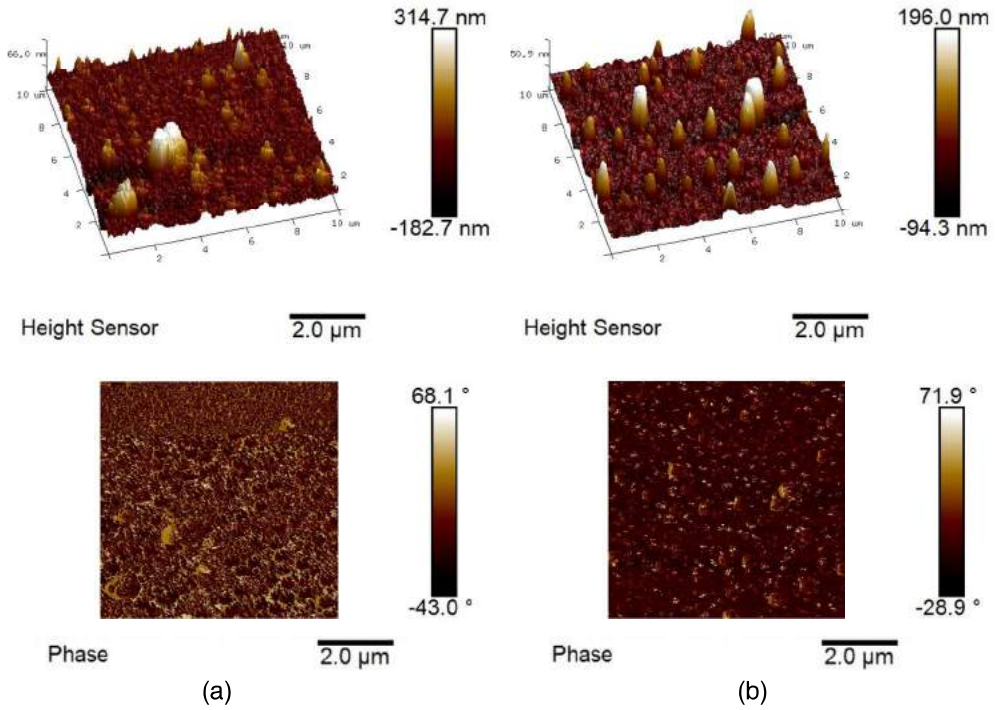

Figure 9: *Height sensor* and *phase* images of substrates at (a) *Stagnant*, and (b) 2.37×10^4 s^{-1} having R_q of 51.75 nm and 32.00 nm, respectively, treated with 0.5 wt.% SDS. The results suggests that SDS is inefficient in removal and rather adsorbs strongly on asphaltene with hydrophobic interactions.

decrease in the surface tension explains the increased removal efficiency of asphaltene from the silica surface.

The fractional volume estimated, as per equation 2, is 0.79 and 0.30 for SDS and CTAB, respectively, that denotes higher removal efficiency achieved with the cationic surfactant. In short, our results suggest that a cationic surfactant in water effectively removes a negatively charged asphaltene surface adsorbed on silica more efficiently than an anionic surfactant.

4. Conclusions

In the current study, we investigated the efficiency of asphaltene removal using the hydrodynamic forces with pH-controlled experiments and ionic sur-

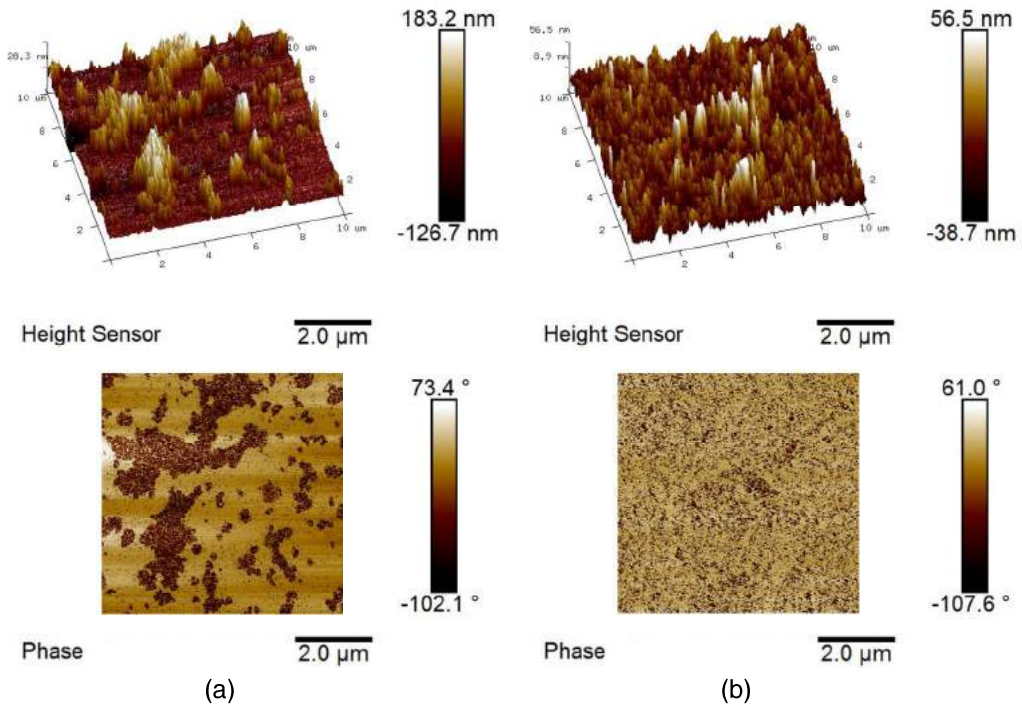

Figure 10: *Height sensor* and *phase* images of substrates at (a) *Stagnant*, and (b) 2.37×10^4 s^{-1} having R_q = 39.40 nm and 12.30 nm, respectively, treated with 0.4 wt.% CTAB. The results suggests that CTAB effectively removes asphaltene from the surface.

factants in water. The removal efficiency increases proportionally with hydrodynamic forces but is also affected by electrostatic double-layer charges in the system defined by zeta potentials. In our study, the asphaltenes exhibit zeta potentials from positive to negative over a pH range of 2 to 10. The iso-electric point (IEP) exists at pH 5.2. The clean glass slides are negatively charged in the entire pH range (Andrade et al., 2009).

The deposition occurs on clean glass slides from an asphaltene dispersion in *n*-heptane, confirmed by an increase in roughness and visible depositions in the AFM images. The shear rates are varied from 0 - 2.37×10^4 s^{-1}, observing a total of six flow states. The observations are for pH 2 to pH 10. However, flow experiments are performed only at pH 5.2, 7, 8.5, and 10. Ionic surfactants, SDS and CTAB, are dissolved in water at neutral pH, and

a separate experiment set is observed in the flow channel. We express our results as parameters of roughness and fractional volume of asphaltene on the surface. To summarize the significant findings of our current study:

- On contacting the asphaltene substrates with water, we observed changes in morphology are affected by charges on asphaltene as well as silica. The oppositely charged asphaltene and silica surface in an acidic medium result in large asphaltene aggregates. As the system moves towards alkalinity, these aggregates disintegrate due to electrostatic repulsion from neighboring asphaltenes and the surface.

- At extreme pH values, the excess H^+ and OH^- ions forms hydrogen bonds with the asphaltene functional groups (Guo et al., 2020) and increases the asphaltene's hydrophilicity. The increased diffusion of water molecules thus causes enhanced swelling of asphaltene aggregates on the surface.

- The removal efficiency increases proportionally with the hydrodynamic forces. The asphaltene removal is promoted by disruption of -NH and -OH bonds between asphaltene and surface (Keshavarz et al., 2019a,b). The repulsion between similarly charged asphaltene and silica surfaces enhances towards higher pH values, resulting in increased asphaltene removal efficiency (Liu et al., 2020). We compared the fractional volume of asphaltene at no-flow to that at the maximum shear rate, which is around 0.12 at pH 10, suggesting asphaltene was significantly removed from the surface.

- The anionic surfactant SDS further increases the zeta potential of asphaltene in water (pH 7) in the negative direction. However, we observed that the asphaltene firmly adheres to the surface. The roughness shows a marginal decline at *Stagnant* state due to the separation of some of the asphaltene aggregates. The stable adsorption of SDS with hydrophobic interactions with asphaltene results in inadequate removal from the surface (Salmón-Vega et al., 2012). Indeed, an increase in hydrodynamic forces causes partial removal of asphaltene from the surface; the roughness is higher than a no-surfactant system in the parallel plate channel.

- The adsorption of CTAB on asphaltene and silica renders both a net positive charge (Kwon et al., 2018). The interfacial tension between

asphaltene and water reduces (Singh, 1999), and asphaltene desorption occurs from the surface by entrapment within the CTAB micellar structure (Rogel et al., 2001). The efficiency increases as the shear rates increase.

The study focused on enhanced oil recovery during water flooding and asphaltene removal in heavier crude oil reservoirs. We described that the removal efficiency is affected by hydrodynamic forces and the zeta potential of asphaltene and mineral surfaces. We conclude that increasing the pH should result in higher asphaltene removal, and that the ionic surfactant should be of opposite charge to that of asphaltene in the system. It is vital to note that asphaltene origin and mineral surface type might affect the extent of removal, as stated here. The interaction forces between asphaltene and surface might differ in the case of asphaltenes that have a different composition of heteroatoms (Taheri-Shakib et al., 2019a,b). In the scope of further study, one can compare the asphaltene removal efficiency with several other surfactants with varying alkyl chain lengths and the mixture of non-ionic and ionic surfactants. One can also observe the effect of surfactants with pH-adjusted aqueous media. Such study's motivation comes from the combined effect of zeta potential and change in interfacial tension.

CRediT Author Statement

Syed Haider Abbas Rizvi: Conceptualization, Methodology, Writing – Original Draft, Visualization, Validation, Investigation. **Shrimali Jonit Bharatbhai:** Methodology, Formal analysis, Writing – Original Draft. **Shivam Gupta:** Methodology, Formal analysis. **Jyoti Phirani:** Writing - Review & Editing, Funding acquisition. **Vikram Singh:** Conceptualization, Supervision, Writing - Review & Editing, Funding acquisition.

Funding Sources

Shell Technology Centre Bangalore, India, financially supported the work.

Declaration of Interest Statement

The authors declare no competing financial interest.

Author Information

Corresponding Author Prof. Vikram Singh Block II-377, Department of Chemical Engineering, Indian Institute of Technology Delhi, Hauz Khas, New Delhi, India - 110016 Email: vs225@chemical.iitd.ac.in (Vikram Singh)

Acknowledgement

The authors gratefully acknowledge Sudip K. Pattanayek (Professor, Department of Chemical Engineering, IIT Delhi), Jayati Sarkar (Professor, Department of Chemical Engineering, IIT Delhi), Ashok N. Baskarwar (Professor, Department of Chemical Engineering, IIT Delhi), and Sujin B. Babu (Professor, Department of Physics, IIT Delhi) for their support in rigorous improvement of the work. We are thankful to the Nanoscale Research Facility to conduct AFM imaging of the samples, Macromolecules and Interfaces Laboratory for contact angle measurements at the Indian Institute of Technology, Delhi. The authors thank Shalini Shikha, Mohit Tiwari, and Asad Abbas for their assistance during experiments.

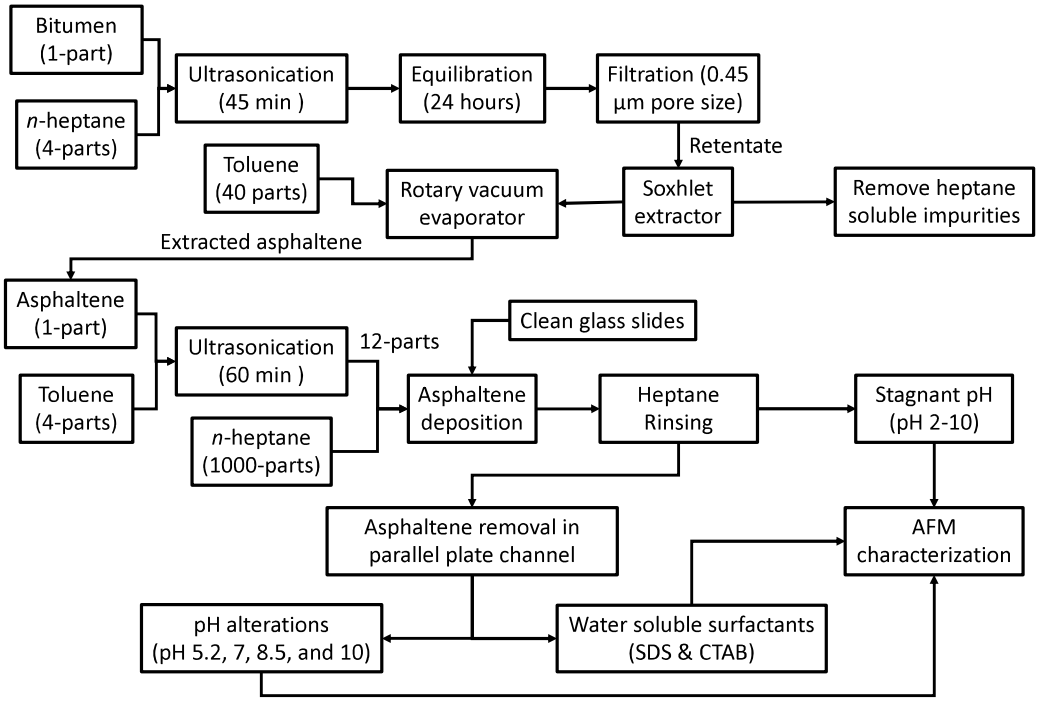

Figure A.11: Process flow diagram for the procedures adopted in the study. The process starts with asphaltene extraction from bitumen, and extracted asphaltene are further used during deposition experiments. The effect of water (pH-adjusted) under no-flow and flow in parallel plate channel are observed after rinsing of substrates with heptane. The removal is also observed with surfactants (SDS and CTAB) under flow conditions. The substrates are analyzed with AFM after drying.

For ease of understanding of the reader about the AFM analysis procedures, we have provided detailed information. Here we state the complete procedure for estimating pixel height and total volume occupied by pixels on the surface. This document also contains a few results from Section 3.2 for additional AFM images and volume analysis.

Appendix A. Detailed Process Flow Diagram

Figure A.11 shows the entire procedure adopted in the study. Asphaltene extraction is done in situ from 55% bitumen emulsion with kerosene (Shalibond, provided by STP Ltd). Bitumen is added to n-heptane (HPLC grade, Fisher Scientific) in the ratio 1:40 (w/v), and the mixture is sonicated for 45 min and equilibrated for 24 h. The filtration is done on a 0.45 μm

pore size paper (Whatman), and the retentate on paper is further washed with heptane in the Soxhlet extractor to dissolve the heptane soluble impurities. The content is further diluted with toluene (HPLC grade, Fisher Scientific), and toluene is vaporized in a rotary vacuum evaporator. The leftover black-colored solids (asphaltene) are weighed and properly stored away from moisture until further use. The asphaltene is dispersed in toluene under ultrasonication and immediately added to pure heptane in a beaker where deposition occurs on clean glass slides for 24 h under maintained conditions of temperature and continuous stirring. After the deposition, asphaltene substrates are rinsed with heptane to flush-off unadsorbed asphaltene on the surface. Further experiments with water, as mentioned in the study, are the observed on solvent rinsed substrates. The asphaltene substrates are analyzed with AFM after oven drying.

Appendix B. AFM Cross-section Analysis

Appendix B.1. Determination of pixel height

Figure B.12 shows a model approach to the cross-section analysis of a *Stagnant* substrate. We sketch only three lines of 3 μm each representing divergent morphology regions on the scan to demonstrate the procedure. In the fundamental analysis, the data is representative of 36 lines (3 μm each). We determine the datum or the zero line from a region (—markers), referring to the *phase* image and selecting a region of greater stiffness (lightest contrast) corresponding to a glass slide. Within the region of the green markers, the maximum variation in height is less than a nanometer. The phase angle is also within $\pm 1^{\circ}$, confirming a region of no deposition. The —and —markers are denominations for intermediate and high depositions, respectively.

A 10 μm line on the surface contains 512 pixels, and therefore 36 lines of 3 μm have a total of 5530 pixels. The randomly sketched lines on the surface cover feature representing any asphaltene amount or no deposition; however, regions with scan errors are omitted. The normalization of height distribution of all the pixels with the datum line (zero) assumes that the datum is in a region of no deposition, supported by the *phase* images. This normalization accounts for estimating the relative amount of material (asphaltene) on the surface. The extraction of a datum or the zero point is from the deepest valley corresponding to no deposition. The normalization strategy is as follows. If, for a particular image, the deepest valley lies at -50 nm, then this pixel is set

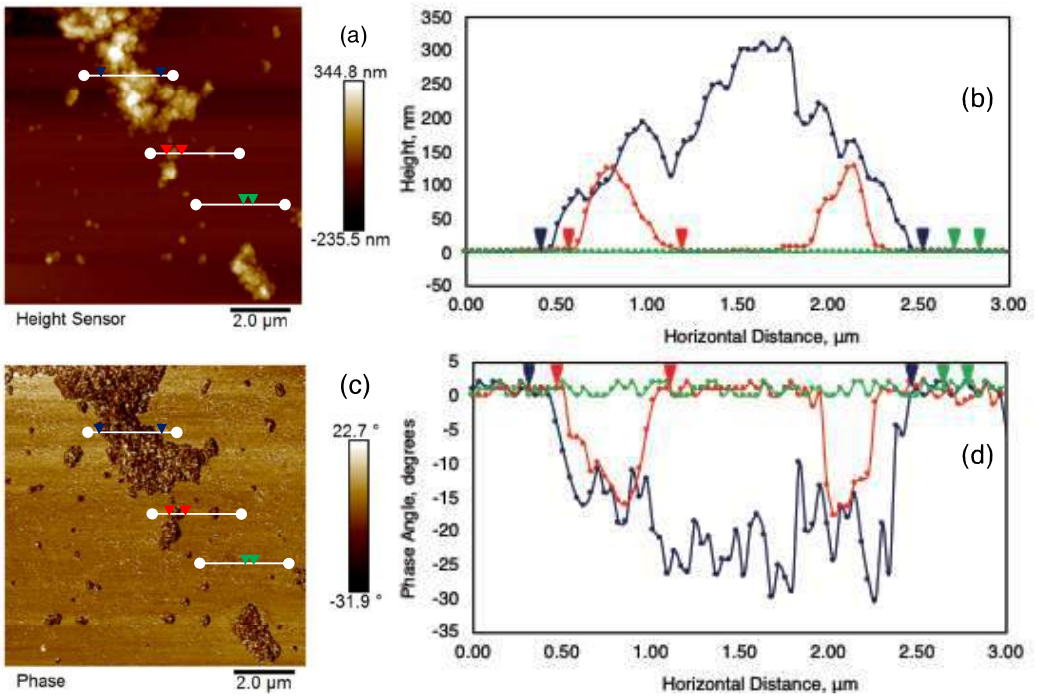

Figure B.12: Cross-section analysis of substrates from the parallel plate channel at *Stagnant* (zero) shear rate: (a) and (c) *Height sensor* and *phase* image with markers at three different regions representing variations in height and phase angles along the line. (b) and (d) graphical representation of height and phase angles of pixels along the line sketched. The markers are at the same location as on the left.

as 0 nm. An increment of +50 nm applies to all of the other pixels as well. The estimation of the height of other features and thickness of deposition is through the adopted procedure.

Appendix B.2. Estimation of aggregate volume on the surface

The volume occupied by a single pixel V_i is calculated from equation B.1.

$$V_i = Z_i \frac{10\mu\text{m} \times 10\mu\text{m}}{512 \times 512} \tag{B.1}$$

where Z_i corresponds to height of the deposited asphaltene on pixel 'i'. The total volume V_t of asphaltene deposited on 5530 pixels of the cross-sectional analysis is calculated as,

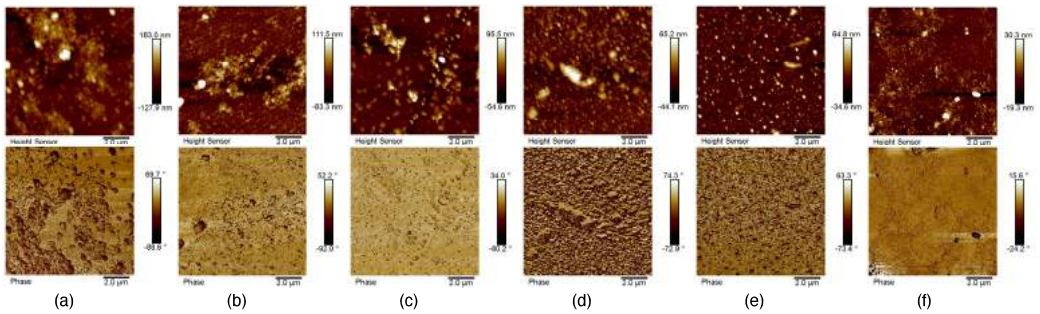

Figure C.13: *Height sensor* and *phase* images of heptane rinsed substrates subjected to various shear rates in the parallel plate channel at pH 10: (a) *Stagnant*, (b) 1.23×10^3 s^{-1}, (c) 3.03×10^3 s^{-1}, (d) 5.46×10^3 s^{-1}, (e) 1.69×10^4 s^{-1}, (f) 2.37×10^4 s^{-1}.

$$V_t = \sum_{1}^{5530} V_i \tag{B.2}$$

We further normalize the total volume at a specific pH with respect to volume of asphaltene ($V_t|_{pH7}$) deposited on the substrate at zero shear rate. The total normalized volume at a shear rate is given by,

$$\bar{V_t} = V_t/V_t|_{pH7} \tag{B.3}$$

The above expression for $\bar{V_t}$ in equation 1 is worked out for calculating volume at each shear rate for pH values of 5.2, 7, 8.5, and 10. We estimate the reduction in volume $\bar{V}_{t_{reduction}}$, as the ratio of the total volume of asphaltene at the maximum shear rate to that at the *Stagnant* for the same pH value.

$$\bar{V}_{t_{reduced}} = 1 - \frac{\bar{V_t}|_{maxshear}}{\bar{V_t}|_{Stagnant}} \tag{B.4}$$

Appendix C. Additional results from the article

The AFM *height sensor* and *phase* images of substrates under hydrodynamic forces at pH 10 are shown in Figure C.13.

Figure C.14 shows plots the normalized volume $\bar{V_t}$, calculated from equation 1 subjected to hydrodynamic forces in the parallel plate channel at pH 5.2, 7, 8.5, and 10.

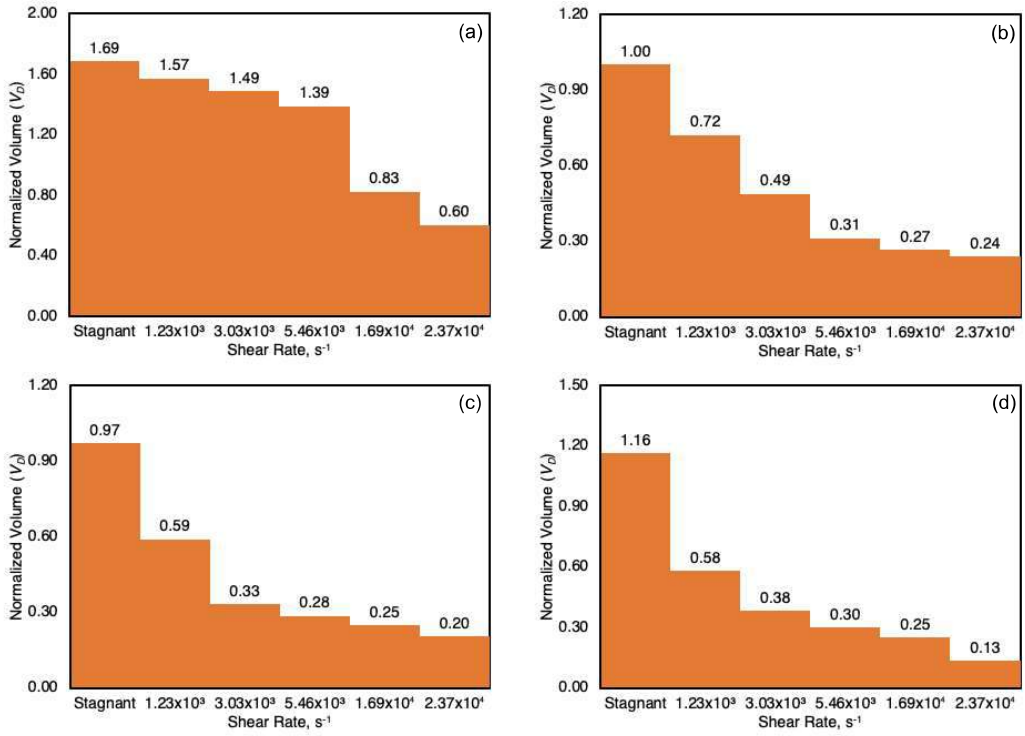

Figure C.14: Normalized volume of aggregates as a function of shear rates at: (a) pH 5.2, (b) pH 7, (c) pH 8.5, and (d) pH 10.

References

Abbas Rizvi, S.H., Yadav, A., Phirani, J., Singh, V., 2021. Deposition and Removal Studies of Asphaltene from the Glass Surface. Energy and Fuels 35, 3228–3239. doi:10.1021/acs.energyfuels.0c03881.

Abraham, T., Christendat, D., Karan, K., Xu, Z., Masliyah, J., 2002. Asphaltene - Silica interactions in aqueous solutions: Direct force measurements combined with electrokinetic studies. Industrial and Engineering Chemistry Research 41, 2170–2177. doi:10.1021/ie0107690.

Ahmadi, M., Chen, Z., 2020. Molecular Interactions between Asphaltene and Surfactants in a Hydrocarbon Solvent: Application to Asphaltene Dispersion. Symmetry 12, 1767. doi:10.3390/sym12111767.

Al-Sahhaf, T.A., Fahim, M.A., Elkilani, A.S., 2002. Retardation of asphaltene precipitation by addition of toluene, resins, deasphalted oil and surfactants. Fluid Phase Equilibria 194-197, 1045–1057. doi:10.1016/S0378-3812(01)00702-6.

Al Sultan, A., Zirrahi, M., Hassanzadeh, H., Abedi, J., 2018. Effect of the Surfactant on Asphaltene Deposition on Stainless-Steel and Glass Surfaces. Energy and Fuels 32, 5635–5642. doi:10.1021/acs.energyfuels.8b00215.

Alboudwarej, H., Beck, J., Svrcek, W.Y., Yarranton, H.W., Akbarzadeh, K., 2002. Sensitivity of asphaltene properties to separation techniques. Energy and Fuels 16, 462–469. doi:10.1021/ef010213p.

Alcázar-Vara, L.A., 2016. Application of Multifunctional Agents During Enhanced Oil Recovery, in: Zamudio-Rivera, L.S. (Ed.), Chemical Enhanced Oil Recovery (cEOR) - a Practical Overview. IntechOpen, Rijeka. chapter 4, pp. 122–145. doi:10.5772/64792.

Andrade, A.L., Souza, D.M., Pereira, M.C., Fabris, J.D., Domingues, R.Z., 2009. Synthesis and characterization of magnetic nanoparticles coated with silica through a sol-gel approach. Cerâmica 55, 420–424. doi:10.1590/s0366-69132009000400013.

Chang, C.L., Fogler, H.S., 1994. Stabilization of Asphaltenes in Aliphatic Solvents Using Alkylbenzene-Derived Amphiphiles. 1. Effect of the Chemical Structure of Amphiphiles on Asphaltene Stabilization. Langmuir 10, 1749–1757. doi:10.1021/la00018a022.

Cheng, S., Bryant, R., Doerr, S.H., Rhodri Williams, P., Wright, C.J., 2008. Application of atomic force microscopy to the study of natural and model soil particles. Journal of Microscopy 231, 384–394. doi:10.1111/j.1365-2818.2008.02051.x.

Collini, H., Li, S., Jackson, M.D., Agenet, N., Rashid, B., Couves, J., 2020. Zeta potential in intact carbonates at reservoir conditions and its impact on oil recovery during controlled salinity waterflooding. Fuel 266, 116927. URL: https://www.sciencedirect.com/science/article/pii/S0016236119323208, doi:https://doi.org/10.1016/j.fuel.2019.116927.

Elsharkawy, A.M., Yarranton, H.W., Al-sahhaf, T.A., Fahim, M.A., 2008. Water-in-crude oil emulsions in the Burgan oilfield: Effects of oil aromaticity, resins to asphaltenes content (R/(R+ a)), and water pH. Journal of Dispersion Science and Technology 29, 224–229.

Eskin, D., Mohammadzadeh, O., Akbarzadeh, K., Taylor, S.D., Ratulowski, J., 2016. Reservoir impairment by asphaltenes: A critical review. The Canadian Journal of Chemical Engineering 94, 1202–1217.

Fakher, S., Ahdaya, M., Elturki, M., Imqam, A., 2020. Critical review of asphaltene properties and factors impacting its stability in crude oil. Journal of Petroleum Exploration and Production Technology 10, 1183–1200. doi:10.1007/s13202-019-00811-5.

Gharbi, K., Benyounes, K., Khodja, M., 2017. Removal and prevention of asphaltene deposition during oil production: A literature review. Journal of Petroleum Science and Engineering 158, 351–360. doi:10.1016/j.petrol.2017.08.062.

Golsefatan, A., Shahbazi, K., 2020. Predicting the effect of nanocomposites on asphaltene removal using a comprehensive approach. Petroleum Science and Technology 38, 64–73. doi:10.1080/10916466.2019.1656241.

Grijalva-Monteverde, H., Arellano-Tánori, O.V., Valdez, M.A., 2005. Zeta potential and langmuir films of asphaltene polar fractions. Energy and Fuels 19, 2416–2422. doi:10.1021/ef050120y.

Gu, Y., Li, D., 2000. The ζ-potential of glass surface in contact with aqueous solutions. Journal of Colloid and Interface Science 226, 328–339. doi:10.1006/jcis.2000.6827.

Guo, J., Zhou, L., Zen, A., Michaelides, A., Wu, X., Wang, E., Xu, L., Chen, J., 2020. Hydration of NH4+ in Water: Bifurcated Hydrogen Bonding Structures and Fast Rotational Dynamics. Physical Review Letters 125, 106001. doi:10.1103/PhysRevLett.125.106001.

Hashmi, S.M., Firoozabadi, A., 2016. Effective removal of asphaltene deposition in metal-capillary tubes. SPE Journal 21, 1747–1754. doi:10.2118/166404-PA.

Ihtsham Hashmi, M., Ghosh, B., 2015. Dynamic asphaltene deposition control in pipe flow through the application of DC potential. Journal of Petroleum Exploration and Production Technology 5, 99–108. doi:10.1007/s13202-014-0113-2.

Indo, K., Ratulowski, J., Dindoruk, B., Gao, J., Zuo, J., Mullins, O.C., 2009. Asphaltene Nanoaggregates Measured in a Live Crude Oil by Centrifugation. Energy & Fuels 23, 4460–4469. doi:10.1021/ef900369r.

Joonaki, E., Buckman, J., Burgass, R., Tohidi, B., 2019. Water versus Asphaltenes; Liquid–Liquid and Solid–Liquid Molecular Interactions Unravel the Mechanisms behind an Improved Oil Recovery Methodology. Scientific Reports 9, 11369. doi:10.1038/s41598-019-47782-5.

Kar, T., Naderi, K., Firoozabadi, A., 2020. Asphaltene Deposition and Removal in Flowlines and Mitigation by Effective Functional Molecules. SPE Journal 25, 771–787. doi:10.2118/199878-PA.

Kesarwani, H., Sharma, S., Mandal, A., 2021. Application of Novel Colloidal Silica Nanoparticles in the Reduction of Adsorption of Surfactant and Improvement of Oil Recovery Using Surfactant Polymer Flooding. ACS Omega 6, 11327–11339. doi:10.1021/acsomega.1c00296.

Keshavarz, V., Khosravanian, R., Taheri-Shakib, J., Salimidelshad, Y., Hosseini, S.A., 2019a. Chemical removal of organic precipitates deposition from porous media: Characterizing adsorption and surface properties. Journal of Petroleum Science and Engineering 175, 200–214. doi:10.1016/j.petrol.2018.12.021.

Keshavarz, V., Taheri-Shakib, J., Khosravanian, R., Hosseini, S.A., Salimidelshad, Y., Saadati, P., 2019b. Experimental investigation of rock-solvent interaction on the properties of carbonate reservoir rock. Journal of Petroleum Science and Engineering 181. doi:10.1016/j.petrol.2019.106246.

Kord, S., Mohammadzadeh, O., Miri, R., Soulgani, B.S., 2014. Further investigation into the mechanisms of asphaltene deposition and permeability impairment in porous media using a modified analytical model. Fuel 117, 259–268. doi:10.1016/j.fuel.2013.09.038.

Kumar, K., Dao, E.K., Mohanty, K.K., 2008. Atomic Force Microscopy Study of Wettability Alteration by Surfactants. SPE Journal 13, 137–145. doi:10.2118/93009-PA.

Kwon, E.H., Go, K.S., Nho, N.S., Kim, K.H., 2018. Effect of Alkyl Chain Length of Ionic Surfactants on Selective Removal of Asphaltene from Oil Sand Bitumen. Energy and Fuels 32, 9304–9313. doi:10.1021/acs.energyfuels.8b01933.

Leon, O., Rogel, E., Torres, G., Lucas, A., 2000. Electrophoretic mobility and stabilization of asphaltenes in low conductivity media. Petroleum Science and Technology 18, 913–927. doi:10.1080/10916460008949882.

León, O., Rogel, E., Urbina, A., Andújar, A., Lucas, A., 1999. Study of the Adsorption of Alkyl Benzene-Derived Amphiphiles on Asphaltene Particles. Langmuir 15, 7653–7657. doi:10.1021/la9812370.

LI, C., WANG, J.q., SHI, B., DENG, W.a., ZHANG, L.l., QUE, G.h., 2008. Effects of active additives on Zeta potential of Lungu atmospheric residue. Journal of Fuel Chemistry and Technology 36, 55–59. doi:10.1016/s1872-5813(08)60012-2.

Li, P., Ishiguro, M., 2016. Adsorption of anionic surfactant (sodium dodecyl sulfate) on silica. Soil Science and Plant Nutrition 62, 223–229. doi:10.1080/00380768.2016.1191969.

Liu, F., Yang, H., Chen, T., Zhang, S., Yu, D., Chen, Y., Xie, Q., 2020. Direct Evidence of Salinity and pH Effects on the Interfacial Interactions of Asphaltene-Brine-Silica Systems. Molecules 25, 1214. doi:10.3390/molecules25051214.

Long, J., Xu, Z., Masliyah, J.H., 2007. Single molecule force spectroscopy of asphaltene aggregates. Langmuir 23, 6182–6190. doi:10.1021/la063764m.

Lv, P., Liu, Y., Zhang, Y., Sun, L., Meng, X., Meng, X., Zou, J., 2020. Optimization of non-ionic surfactants for removing emulsified oil from gas condensate oil–water emulsion in N oilfield. Journal of Petroleum Exploration and Production Technology 10, 3025–3030. doi:10.1007/s13202-020-00950-0.

Madhi, M., Kharrat, R., Hamoule, T., 2018. Screening of inhibitors for remediation of asphaltene deposits: Experimental and modeling study. Petroleum 4, 168–177. doi:10.1016/j.petlm.2017.08.001.

Miadonye, A., Evans, L., 2010. The solubility of asphaltenes in different hydrocarbon liquids. Petroleum Science and Technology 28, 1407–1414. doi:10.1080/10916460902936960.

Mitchell, D.L., Speight, J.G., 1973. The solubility of asphaltenes in hydrocarbon solvents. Fuel 52, 149–152. doi:10.1016/0016-2361(73)90040-9.

Mullins, O.C., Sabbah, H., Eyssautier, J., Pomerantz, A.E., Barré, L., Andrews, A.B., Ruiz-Morales, Y., Mostowfi, F., McFarlane, R., Goual, L., Lepkowicz, R., Cooper, T., Orbulescu, J., Leblanc, R.M., Edwards, J., Zare, R.N., 2012. Advances in asphaltene science and the Yen-Mullins model. Energy and Fuels 26, 3986–4003. doi:10.1021/ef300185p.

Neil, B.O., Maley, D., Lalchan, C., Well, T., 2015. Prevention of Acid Induced Asphaltene Precipitation : A Comparison of Anionic vs . Cationic Surfactants. Journal of Canadian Petroleum Technology 54, 49–62.

Neves, G.B., de Sousa, M.d.A., Travalloni-Louvisse, A.M., Lucas, E.F., Gonz´lez, G., 2001. Characterization of asphaltene particles by light scattering and electrophoresis. Petroleum Science and Technology 19, 35–43. doi:10.1081/LFT-100001225.

Ok, S., Mahmoodinia, M., Rajasekaran, N., Sabti, M.A., Lervik, A., van Erp, T.S., Cabriolu, R., 2019. Molecular Structure and Solubility Determination of Asphaltenes. Energy and Fuels 33, 8259–8270. doi:10.1021/acs.energyfuels.9b01737.

Parra-Barraza, H., Hernández-Montiel, D., Lizardi, J., Hernández, J., Herrera Urbina, R., Valdez, M.A., 2003. The zeta potential and surface properties of asphaltenes obtained with different crude oil/n-heptane proportions. Fuel 82, 869–874. doi:10.1016/S0016-2361(03)00002-4.

Poteau, S., Argillier, J.F., Langevin, D., Pincet, F., Perez, E., 2005. Influence of pH on stability and dynamic properties of asphaltenes and other amphiphilic molecules at the oil-water interface. Energy and Fuels 19, 1337–1341. doi:10.1021/ef0497560.

Pradilla, D., Subramanian, S., Simon, S., Sjöblom, J., Beurroies, I., Denoyel, R., 2016. Microcalorimetry Study of the Adsorption of Asphaltenes and Asphaltene Model Compounds at the Liquid-Solid Surface. Langmuir 32, 7294–7305. doi:10.1021/acs.langmuir.6b00816.

Rajagopal, K., Silva, S.M., 2004. An experimental study of asphaltene particle sizes in n-heptane-toluene mixtures by light scattering. Brazilian Journal of Chemical Engineering 21, 601–609. doi:10.1590/S0104-66322004000400009.

Rapp, M.V., Donaldson, S.H., Gebbie, M.A., Gizaw, Y., Koenig, P., Roiter, Y., Israelachvili, J.N., 2015. Effects of Surfactants and Polyelectrolytes on the Interaction between a Negatively Charged Surface and a Hydrophobic Polymer Surface. Langmuir 31, 8013–8021. doi:10.1021/acs.langmuir.5b01781.

Ratnakar, R.R., Mantilla, C.A., Dindoruk, B., 2020. Impact of Asphaltenes on Contact-Angle Variations and Surface Topography and Composition. SPE Journal 25, 1082–1095. doi:10.2118/190385-PA.

Rogel, E., Leon, O., Espidel, Y., Gonzalez, Y., 2001. Asphaltene Stability in Crude Oils. SPE Production & Facilities 16, 84–88. doi:10.2118/72050-PA.

Rui, Z., Wang, X., Zhang, Z., Lu, J., Chen, G., Zhou, X., Patil, S., 2018. A realistic and integrated model for evaluating oil sands development with Steam Assisted Gravity Drainage technology in Canada. Applied Energy 213, 76–91. doi:10.1016/j.apenergy.2018.01.015.

Salehzadeh, M., Akherati, A., Ameli, F., Dabir, B., 2016. Experimental study of ultrasonic radiation on growth kinetic of asphaltene aggregation and deposition. Canadian Journal of Chemical Engineering 94, 2202–2209. doi:10.1002/cjce.22593.

Salmón-Vega, S., Herrera-Urbina, R., Lira-Galeana, C., Valdez, M.A., 2012. The effect of ionic surfactants on the electrokinetic behavior of asphaltene from a maya Mexican oil. Petroleum Science and Technology 30, 986–992. doi:10.1080/10916466.2010.495966.

Scheffer, K., Méheust, Y., Carvalho, M.S., Mauricio, M.H.P., Paciornik, S., 2021. Enhancement of oil recovery by emulsion injection: A pore

scale analysis from X-ray micro-tomography measurements. Journal of Petroleum Science and Engineering 198, 108134. doi:10.1016/j.petrol.2020.108134.

Scott, W.W., Bhushan, B., 2003. Use of phase imaging in atomic force microscopy for measurement of viscoelastic contrast in polymer nanocomposites and molecularly thick lubricant films. Ultramicroscopy 97, 151–169. doi:10.1016/S0304-3991(03)00040-8.

Shayan, N.N., Mirzayi, B., 2015. Adsorption and Removal of Asphaltene Using Synthesized Maghemite and Hematite Nanoparticles. Energy and Fuels 29, 1397–1406. doi:10.1021/ef502494d.

Singh, B.P., 1999. The role of surfactant adsorption in the improved dewatering of fine coal. Fuel 78, 501–506.

Sjöblom, J., Hemmingsen, P.V., Kallevik, H., 2007. The Role of Asphaltenes in Stabilizing Water-in-Crude Oil Emulsions, in: Asphaltenes, Heavy Oils, and Petroleomics, pp. 549–587. doi:10.1007/0-387-68903-6-21.

Soleymanzadeh, A., Yousefi, M., Kord, S., Mohammadzadeh, O., 2019. A review on methods of determining onset of asphaltene precipitation. Journal of Petroleum Exploration and Production Technology 9, 1375–1396. doi:10.1007/s13202-018-0533-5.

Soorghali, F., Zolghadr, A., Ayatollahi, S., 2015. Effects of Native and Non-Native Resins on Asphaltene Deposition and the Change of Surface Topography at Different Pressures: An Experimental Investigation. Energy and Fuels 29, 5487–5494. doi:10.1021/acs.energyfuels.5b00366.

Sumner, A.L., Menke, E.J., Dubowski, Y., Newberg, J.T., Penner, R.M., Hemminger, J.C., Wingen, L.M., Brauers, T., Finlayson-Pitts, B.J., 2004. The nature of water on surfaces of laboratory systems and implications for heterogeneous chemistry in the troposphere. Physical Chemistry Chemical Physics , 604–613doi:10.1039/b308125g.

Taheri-Shakib, J., Hosseini, S.A., Kazemzadeh, E., Keshavarz, V., Rajabi-Kochi, M., Naderi, H., 2019a. Experimental and mathematical model evaluation of asphaltene fractionation based on adsorption in porous media: Dolomite reservoir rock. Fuel 245, 570–585. doi:10.1016/j.fuel.2019.02.057.

Taheri-Shakib, J., Keshavarz, V., Kazemzadeh, E., Hosseini, S.A., Rajabi-Kochi, M., Salimidelshad, Y., Naderi, H., Bakhtiari, H.A., 2019b. Experimental and mathematical model evaluation of asphaltene fractionation based on adsorption in porous media: Part 1. calcite reservoir rock. Journal of Petroleum Science and Engineering 177, 24–40. doi:10.1016/j.petrol.2019.02.032.

Taheri-Shakib, J., Rajabi-Kochi, M., Kazemzadeh, E., Naderi, H., Salimidelshad, Y., Esfahani, M.R., 2018. A comprehensive study of asphaltene fractionation based on adsorption onto calcite, dolomite and sandstone. Journal of Petroleum Science and Engineering 171, 863–878. doi:10.1016/j.petrol.2018.08.024.

Taheri-Shakib, J., Saadati, N., Esfandiarian, A., Hosseini, S.A., Rajabi-Kochi, M., 2020a. Characterizing the wax-asphaltene interaction and surface morphology using analytical spectroscopy and microscopy techniques. Journal of Molecular Liquids 302. doi:10.1016/j.molliq.2020.112506.

Taheri-Shakib, J., Zojaji, I., Saadati, N., Kazemzadeh, E., Esfandiarian, A., Rajabi-Kochi, M., 2020b. Investigating molecular interaction between wax and asphaltene: Accounting for wax appearance temperature and crystallization. Journal of Petroleum Science and Engineering 191. doi:10.1016/j.petrol.2020.107278.

Tyrode, E., Rutland, M.W., Bain, C.D., 2008. Adsorption of CTAB on hydrophilic silica studied by linear and nonlinear optical spectroscopy. Journal of the American Chemical Society 130, 17434–17445. doi:10.1021/ja805169z.

Vilas Bôas Fávero, C., Hanpan, A., Phichphimok, P., Binabdullah, K., Fogler, H.S., 2016. Mechanistic Investigation of Asphaltene Deposition. Energy and Fuels 30, 8915–8921. doi:10.1021/acs.energyfuels.6b01289.

Wang, J., Li, C., Zhang, L., Que, G., Li, Z., 2009. The properties of asphaltenes and their interaction with amphiphiles. Energy and Fuels 23, 3625–3631. doi:10.1021/ef801148y.

Wang, J., Song, H., Wang, Y., 2020. Investigation on the micro-flow mechanism of enhanced oil recovery by low-salinity water flooding in carbonate reservoir. Fuel 266, 117156. URL: https://www.sciencedirect.

com/science/article/pii/S0016236120301514, doi:https://doi.org/10.1016/j.fuel.2020.117156.

Yarranton, H.W., 1997. Asphaltene Solubility and Asphaltene Stabilized Water-in-Oil Emulsions. Ph.D. thesis. University of Alberta.

Zhang, L., Xie, L., Shi, C., Huang, J., Liu, Q., Zeng, H., 2017. Mechanistic Understanding of Asphaltene Surface Interactions in Aqueous Media. Energy and Fuels 31, 3348–3357. doi:10.1021/acs.energyfuels.6b02092.

Zojaji, I., Esfandiarian, A., Taheri-Shakib, J., 2021. Toward molecular characterization of asphaltene from different origins under different conditions by means of FT-IR spectroscopy. doi:10.1016/j.cis.2020.102314.